


 Cite this: *RSC Adv.*, 2021, **11**, 33048

Catalytic approach to *in vivo* metabolism of atractylenolide III using biomimetic iron–porphyrin complexes†

 Hanae Lim,^a Hyeri Jeon,^a Seungwoo Hong^{*a} and Jung-Hoon Kim^{ID}^{*b}

Atractylenolide III (AT-III) is a pharmacologically effective phytochemical and is known to be oxygenated during systemic metabolism mainly by cytochrome P450 enzymes (CYP450s), iron-containing porphyrin-based oxygenases. In rat plasma samples, the oxygenated metabolite of orally ingested AT-III was determined using liquid chromatography/mass spectrometry and the oxygenated form of AT-III was maintained at higher levels than the original form of AT-III. *In situ* catalytic reactions using the iron(IV)-oxo porphyrin π -cation radical complex, $[(\text{tmp}^+)\text{Fe}^{\text{IV}}(\text{O})]^+$, demonstrated that both H-atom abstraction and an oxygen rebound mechanism participated in the oxygenation process of AT-III. Density functional theory (DFT) confirmed the oxidative transformation occurred at the 4th and 10th carbon positions of AT-III. Co-treatment with acetaminophen had different effects between *in vivo* and *in situ* models of AT-III metabolism. AT-III was metabolized *via* an oxygenation process in the rat body, where CYP450 and other O_2 -activating metalloenzymes might participate in the metabolism. The present work provided the oxidative metabolism of AT-III using an *in vivo* model parallel with *in situ* biomimetic reaction models.

 Received 29th June 2021
 Accepted 18th September 2021

DOI: 10.1039/d1ra05014a

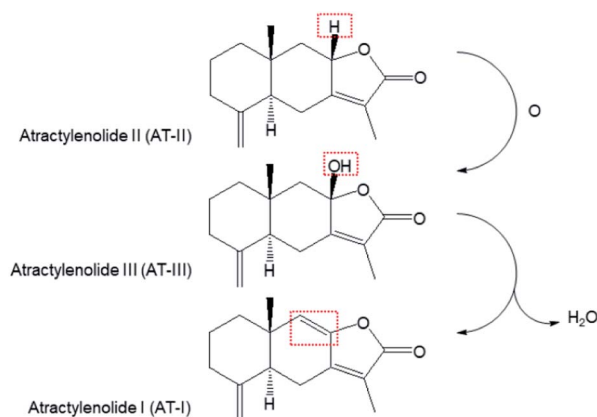
rsc.li/rsc-advances

Introduction

Atractylenolide III (AT-III, $\text{C}_{15}\text{H}_{20}\text{O}_3$, $\text{MW} = 248.32 \text{ g mol}^{-1}$) is a sesquiterpene lactone-type phytochemical mainly derived from *Atractylodes japonica* Koidzumi (Asteraceae), a medicinal plant traditionally used for treating gastrointestinal disorders. AT-III has been recently recognized as an emerging bioactive compound known for its pharmacological effects, such as anticarcinogenic properties,¹ inhibition of muscular atrophy,² microglial neuroprotection,³ and anti-inflammation.⁴ After oral administration, AT-III exerts these biological effects *via* systemic circulation by acting on the target organs or tissues in its original form or after chemical modification *via in vivo* metabolic processes. In our previous study a biomimetic iron(IV)-oxo porphyrin π -cation radical complex (known as

compound I) model has shown that AT-III was oxidised from atractylenolide II ($\text{C}_{15}\text{H}_{20}\text{O}_2$, $\text{MW} = 232.32 \text{ g mol}^{-1}$) and dehydrated to atractylenolide I ($\text{C}_{15}\text{H}_{18}\text{O}_2$, $\text{MW} = 230.3 \text{ g mol}^{-1}$) *via* an intrinsic biosynthetic pathway in *A. japonica* (Scheme 1).⁵ Although AT-III is considered as one of the final products of oxidative metabolism in the plant, it can act as a precursor during *in vivo* drug metabolism after intragastric administration.

Drug metabolism, which is pivotal for modifying a biological substrate's structure, alters the compound's hydro-/electrophilic moieties, increases/decreases toxicity, or changes



Scheme 1 The transformation of atractylenolide I, II, and III in biosynthetic pathway (ref. 5).

^aDepartment of Chemistry, The Research Institute of Natural Sciences, Sookmyung Women's University, 04310, Seoul, Republic of Korea. E-mail: hsw@sookmyung.ac.kr; Fax: +82-2-2077-7321; Tel: +82-2-2077-7829

^bDivision of Pharmacology, School of Korean Medicine, Pusan National University, 50612, Yangsan, Republic of Korea. E-mail: kmsct@pusan.ac.kr; Fax: +81-51-510-8420; Tel: +82-51-510-8456

† Electronic supplementary information (ESI) available: Chromatograms of atractylenolide III/oxidized atractylenolide III and the mass spectra; UV-vis spectral changes of **1** (0.025 mM) observed at -20°C ; plot of pseudo-first order rate constants (k_{obs}); UV-vis spectral changes of $[(\text{tmp}^+)\text{Fe}^{\text{IV}}(\text{O})]^+$ (0.025 mM) (**1**, red line) after the addition of 20 equiv. of APAP at -20°C ; cyclic voltammograms of (a) AT-III (2.0 mM) and (b) APAP (2.0 mM); GC data of the standard samples; chromatogram of oxygenated atractylenolide III and the mass spectra. See DOI: 10.1039/d1ra05014a



its biological activity.⁶ These modifications are caused by oxidation, reduction, and conjugation reactions in the presence of specific enzymes, and occur mainly in the liver.⁷ Among the heme-containing metalloenzymes responsible for drug metabolism, cytochrome P450 isozymes (CYP450s) play a key role in phase I metabolism *via* the oxidative transformation of the exogenous substrate, namely dextromethorphan.⁸ In the catalytic cycle of CYP450-mediated metabolism, the insertion of an oxygen atom in the substrate of interest is essentially mediated by an iron-containing porphyrin (heme), which is a core oxygen-presenting structure of CYP450 enzymes, with the help of the cofactor NADPH.⁹ The exogenous substrate initiates the electron transfer process and the ferric-to-ferrous reduction takes place in order to further react with dioxygen to yield porphyrin π -cation radical (known as compound I). The compound I, a strong oxidant, oxidizes biomolecules and mediates the dissociation of the transformed product.¹⁰ Compound I introduces two crucial metabolic pathways during the CYP450-mediated metabolism process, both of which are initiated by a hydrogen atom abstraction step *via* the hydroxylation or desaturation of the aliphatic groups.¹¹

Various organic substrates have their own oxidation rate constants during their respective oxidation/oxygenation reactions with compound I; these rate constants can be modulated by adjusting experimental conditions such as the temperature and pressure.^{12,13} This has promoted increased interest in the use of synthetic biomimetic model complexes as oxidation catalysts. Researchers are keenly interested in finding chemical probes that can offer mechanistic insights into biological pathways of these oxidation/oxygenation reactions. Previous studies focused on stabilising and characterising compound I have led to breakthroughs in our understanding of the fundamental reaction steps governing the diverse oxidative reactivity of most heme enzymes in the metabolism of chemical drugs.^{14,15} Meanwhile, the oxidative reaction of compound I is also applicable to the *in vivo* metabolism of phytochemicals from natural products.

In this work, *in vivo* studies on the oxygenation of metabolites in plasma samples collected from rats after the oral administration of AT-III were conducted by applying an liquid chromatography/mass spectrometry (LC/MS) method. A biomimetic model such as an iron(IV)-oxo porphyrin π -cation radical complex was utilized to confirm the pathway governing the *in vivo* metabolism of AT-III mediated by CYP450 (Scheme S1†). The oxidation rate of AT-III was calculated and the structure of its oxygenated metabolite was estimated *via* density functional theory (DFT) calculation. Additionally, investigations on the influence of acetaminophen (APAP), which is a widely and frequently used over-the-counter analgesic, on the *in vivo* metabolism and the oxidation rate of AT-III were conducted to provide its synergistic effects.

Results and discussion

Determination of atractylenolide-III and its oxygenated metabolite in the plasma samples

The ionization of the target compounds was performed in positive electrospray ionization mode. A full-scan mode was

applied for detecting AT-III and its metabolite. The molecular ion $[M + H]^+$ of AT-III and its fragmented ions were acquired at m/z of 248.93 ($t_R = 8.3$ min) and its fragmented ions were detected at m/z 230.96 and 163.01 *via* MS² and MS³ analyses (Fig. S1†). After oral administration, the molecular ion of the AT-III metabolite, which had undergone the addition of an oxygen atom (AT-III-O, $t_R = 5.2$ min), was detected at m/z 264.97 in the plasma samples. Further fragmentation was noted at m/z 246.99, 229.13 and 201.09, respectively, as determined *via* MS² and MS³ analyses. These ions contained an extra 16 Da in their original structures, as previously reported (Fig. S2†).¹⁶

In the mean relative area ratio–time profiles, the mean ratio of AT-III decreased for the peak at 0.5 h after oral administration, whereas the intensity of the oxygenated AT-III peaks increased almost threefold relative to the peaks of the original AT-III, regardless of the presence of APAP. These observed increases in the AT-III metabolite relative to the parent AT-III compound were attributed to *in vivo* metabolic amplification since some metabolites of phytochemicals are known to exhibit this behaviour.^{17,18} The relative area ratios of AT-III in the plasma samples between the single and APAP-combined administered groups were not significantly different for all time-courses investigated. The ratio associated with AT-III-O, which exhibited a notable increase at 0.5 h in both groups, also showed statistically insignificant differences between the single and combined administered groups across all time-courses investigated. Even though the mean area under the curve (AUC) of the relative area ratios of AT-III in the single group (1.883 ± 0.311) decreased slightly after co-administration with APAP (1.135 ± 0.288), the differences in the AUCs were not statistically significant. There were no significantly significant differences in the mean AUCs of the relative area ratios of AT-III-O between the single (9.246 ± 1.274) and the APAP-combined (9.015 ± 1.424) groups, respectively (Fig. 1). It was

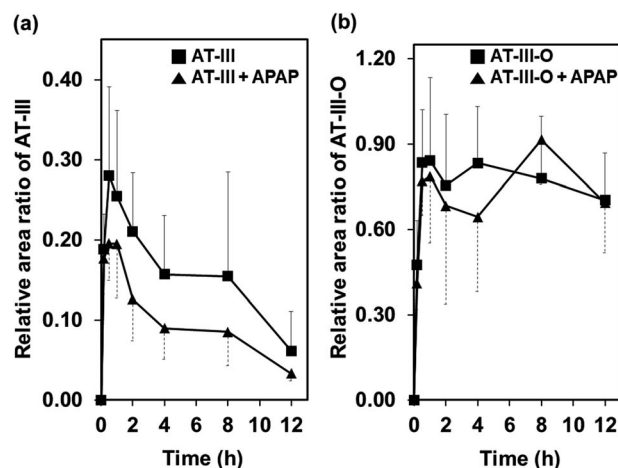


Fig. 1 (a) Mean relative area ratio–time profiles of atractylenolide III (AT-III) and (b) oxygenated atractylenolide III (AT-III-O) after administration of AT-III single or with acetaminophen (APAP). Relative area ratio = the peak area of target compound/the peak area of IS. Differences of relative area ratios between single and combinative administration groups were not statistically significant.



assumed that the influx of AT-III in the animal's circulation system and the production of the oxidative metabolite were both unaffected by the simultaneous administration of APAP.

Oxidative transformation of atractylenolide III using biomimetic model of cytochrome P450

In our previous work, we demonstrated that a high-valent iron(IV)-oxo porphyrin π -cation radical complex, $[(\text{tmp}^+) \text{Fe}^{\text{IV}}(\text{O})]^+$ (**1**) ($\text{tmp} = \text{meso-tetramesitylporphyrin}$), was capable of activating the C–H bond of AT-II to produce AT-III. H-atom abstraction from AT-II generated $[(\text{tmp})\text{Fe}^{\text{IV}}(\text{OH})]$ and the subsequent oxygen rebound process formed AT-III.⁵ In the present study, the analysis of the plasma samples obtained after the single-administration of AT-III and the co-administration of AT-III and APAP revealed that the oxidised product of AT-III had been formed. The addition of AT-III to the $\text{CH}_3\text{CN}/\text{CH}_2\text{Cl}_2$ (9 : 1) solvent mixture containing **1** at -40°C did not afford any spectral changes (Fig. S3,† inset). However, the direct oxidation of AT-III occurred when the reaction temperature was increased to -20°C (Fig. 2).

The natural decay rate was independently calculated as $8.2 \times 10^{-3} \text{ s}^{-1}$ (Fig. S3,† inset). After the addition of 20 equiv. of AT-III to the $\text{CH}_3\text{CN}/\text{CH}_2\text{Cl}_2$ (9 : 1) solvent mixture of **1**, the notably slow decay rate of $1.2 \times 10^{-2} \text{ s}^{-1}$ was observed due to the disappearance of **1** with the concomitant formation of $[\text{Fe}^{\text{III}}(\text{tmp})]^+$ (Fig. 2). The observed decay rate of **1** showed a linear dependence on the AT-III concentration, resulting in a second-order rate constant (k_2) value of $2.8 \text{ M}^{-1} \text{ s}^{-1}$ for the oxidation of AT-III by **1** at -20°C (Fig. S4†). Interestingly, the immediate disappearance of **1** was detected when APAP was used as a substrate, indicating that APAP was more preferentially oxidised than AT-III (Fig. S5†). APAP is known to be oxidised to *N*-acetyl-*p*-benzoquinone-imine (NAPQI), with further conversion to benzoquinone.¹⁹ Since both AT-III and APAP could be competently oxidised by **1**, their electrochemical properties were examined *via* cyclic voltammetry (Fig. S6†). The

increased intensity of the oxidation peak potential of AT-III was $\sim 0.25 \text{ V vs. Ag/Ag}^+$, whereas that of APAP was $-0.50 \text{ V vs. Ag/Ag}^+$. This clearly demonstrated that APAP was much easier to be oxidised than AT-III, thereby accounting for the differences in their redox reactivity originating from their electrochemical properties. The proposed mechanism of APAP oxidation indicated that the proton-coupled electron transfer process was surmised to be the rate-determining step for the production of NAPQI.¹⁹ For AT-III oxidation, the oxygenation reaction could occur *via* the H-atom abstraction process, followed by the oxygen rebound mechanism.⁵ As the electron transfer reaction occurred, smaller structural changes were noted in **1** than in the group transfer reaction because the oxidation of APAP would require less energetic barrier than that of AT-III.²⁰ Thus, the reaction between **1** and APAP was preferentially promoted compared to its counterpart with AT-III.

Confirmation of oxygenated positions at AT-III using density functional theory (DFT) calculation

Gas chromatography analysis of the organic products, which was conducted after the completion of the reaction between **1** and AT-III, showed a new peak with a retention time at 21.3 min that was assigned to the oxidised product of AT-III (Fig. S7†). However, the peak at 21.3 min did not appear when APAP and AT-III were introduced simultaneously; instead, a new peak attributed to NAPQI was detected at a retention time of 18.3 min, clearly indicating that the presence of APAP in the reaction solution hindered the oxygenation of AT-III by **1**. Even though gas chromatography/mass spectrometry (GC/MS) analysis suggested that an oxygen atom was incorporated into the product, the isolation and recrystallization of this organic product was unsuccessful. Alternatively, DFT-calculations for all possible oxygenated products were conducted to determine the optimised structures for the organic products and to simulate plausible positions for oxygenation on the AT-III molecule. The higher spin density on the carbon atoms at the 4th and 10th positions of the oxidised AT-III indicated that these carbons were more basic and, thus, highly prone to oxidation (Fig. 3a). We then calculated the relative energy of radical species of the corresponding radicals on 4th and 10th position; the energy of radical on 10th position of AT-III was $12.68 \text{ kcal mol}^{-1}$ higher than that on 4th position (Fig. 3b and Table 1). Therefore, we suggested that the hydroxylation would occur at 4th position of AT-III. Given these findings, two oxygenated structures of AT-III

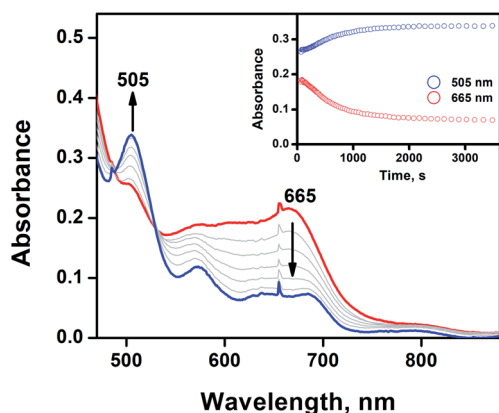


Fig. 2 UV-vis spectral changes of $[(\text{tmp}^+) \text{Fe}^{\text{IV}}(\text{O})]^+$ (0.025 mM) (**1**, red line) upon addition of 20 equiv. of AT-III at -20°C , resulting in the formation of $[\text{Fe}^{\text{III}}(\text{tmp})](\text{CF}_3\text{SO}_3)$ (blue line). Inset shows the time course of the formation of $[\text{Fe}^{\text{III}}(\text{tmp})](\text{CF}_3\text{SO}_3)$ (blue dot) and the decay of **1** (red dot) monitored at 505 and 665 nm, respectively.

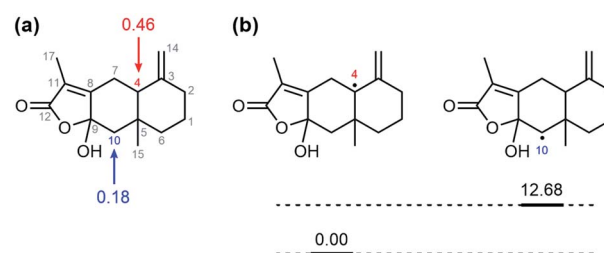


Fig. 3 (a) Mulliken spin densities of one electron oxidized AT-III. (b) The relative energies diagram of radical on 4th and 10th carbon.



Table 1 Relative energies in kcal mol⁻¹

	ΔE_{6-31G}	$\Delta \Delta E_{6-311+G^{**}}$	ΔE^a	$\Delta \Delta Z_0$	$\Delta \Delta E_{\text{thermal}}^b$	$-T\Delta \Delta S^b$	$\Delta \Delta \text{Disp}$	ΔG^c
4th Carbon oxidized AT-III	0.00	0.00	0.00	0.00	0.00	0.00	0.00	0.00
10th Carbon oxidized AT-III	1.56	-0.73	0.83	0.32	0.06	-0.20	0.59	1.60
Radical on 4th carbon of AT-III	0.00	0.00	0.00	0.00	0.00	0.00	0.00	0.00
Radical on 10th carbon of AT-III	13.00	-0.32	12.68	-0.34	0.06	0.39	-0.41	12.38

^a Electronic energy, sum of the previous two columns. ^b $T = 298$ K. ^c Sum of the five previous columns, $\Delta G = \Delta E + \Delta \Delta Z_0 + \Delta \Delta E_{\text{thermal}} - T\Delta \Delta S + \Delta \Delta \text{Disp}$.

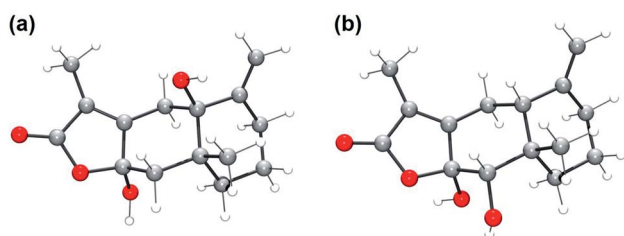


Fig. 4 DFT-optimized structures of (a) 4th carbon and (b) 10th carbon oxidized AT-III. O, red; C, gray; H, white.

were envisioned (Fig. 4). Analysis showed that their relative energies differed by only 1.49 kcal mol⁻¹, indicating that both positions were susceptible to be hydroxylated (Table 1).

LC/MS analysis revealed the presence of three distinct peaks in the oxidised by-product of AT-III after the reaction with **1** (Fig. S8a†). One ($t_R = 5.3$ min) of these peaks, which produced a molecular ion observed at m/z 265.00, fragmented to m/z of 246.95, 229.12 and 201.06, respectively, as noted *via* MS² and MS³ analyses. The molecular ion and its fragmented ions were noted as the addition of an oxygen atom (16 Da), and their associated spectra matched those of AT-III-O in the plasma samples after oral administration (Fig. S8b-d†). These results clearly provided the evidence that enzymes bearing an iron(IV)-oxo porphyrin, particularly the CYP450 enzymes, were responsible for the *in vivo* oxidative metabolism of ingested AT-III. The difference noted between the relative sizes of the peak observed at 5 min and the two peaks at 6 min were reversed in the plasma samples (Fig. S2a†), as the latter peaks were barely detected in the rat plasma samples due to lower detection sensitivity.

Experimental

Chemicals and reagents

Analytical-grade methanol and ethyl acetate were purchased from J.T. Baker Inc. (Phillipsburg, NJ, USA). LC/MS-grade acetonitrile and water containing 0.1% formic acid were purchased from Fisher Scientific (Pittsburgh, PA, USA). Atractylenolide III (AT-III) was purchased from ChemFace (Wuhan, Hubei, China). As the internal standard (IS), fraxinellone was purchased from Chengdu Biopurify Phytochemicals Ltd. (Chengdu, Sichuan, China). Acetonitrile (CH₃CN) and dichloromethane (CH₂Cl₂) were dried according to reported procedures and distilled under Ar prior to use.²¹ *m*-Chloroperbenzoic acid (*m*-CPBA) was purified by washing with

phosphate buffer (pH 7.4), followed by water and then dried under reduced pressure. [Fe^{III}(tmp)]Cl was purchased from Frontier Scientific Inc. (Logan, UT, USA). [Fe^{III}(tmp)](CF₃SO₃) was prepared by stirring equimolar amounts of [Fe^{III}(tmp)]Cl and AgCF₃SO₃, followed by filtration through a 0.45 mm filter. The resulting solution was used immediately.

Animals

Male Sprague Dawley (SD) rats (196.06 ± 7.61 g) were supplied by Samtako (Incheon, Korea). The SD rats were housed at constant temperature (22 ± 2 °C) and relative humidity (50 ± 10%) under a 12 h light/dark cycle for 7 days with free access to feed and water before the experiments. After an overnight fasting period, AT-III was administered to the rats intragastrically. Animal experiments were conducted per the guidelines for animal experimentation issued by Pusan National University. The experimental procedures were approved beforehand by the Animal Ethics Committee of Pusan National University (PNU-2020-2488).

LC/MS conditions

An Accela LC system (Thermo Fisher Scientific, MA, USA) equipped with an autosampler, degasser, and quaternary solvent pump was used for the detection of AT-III and its metabolites. The compounds were separated on a Hypersil GOLD C₁₈ column (2.1 mm × 100 mm, 1.9 μm; Thermo Fisher Scientific, MA, USA) at 35 °C. A flow rate was set at 300 μL min⁻¹ with an injection volume of 5.0 μL. The aqueous mobile phase was optimised by using 0.1% formic acid and 10 mM ammonium acetate (pH 3.5 with formic acid); the peak of AT-III was only detected in the presence of 0.1% formic acid. Therefore, 0.1% formic acid was chosen as a modifier for the aqueous mobile phase (v/v). Compared to the adamantyl functional group (ADME) column, the octadecylsilane (C₁₈)-coated column offered better sensitivity and improved the peak shape of AT-III. The mobile phase consisted of water (containing 0.1% formic acid, A) and acetonitrile (B); the gradient elution applied was as follows: 7% (B) for 0–1 min, 70–85% (B) for 1–10 min, 85% (B) for 10–11 min, followed by equilibrated to 7% (B) until the end of the analysis.

An LCQ Fleet ion-trap mass spectrometer (Thermo Fisher Scientific, MA, USA) was used to detect compounds in the eluent using an electrospray ionisation source in the positive-ion mode. The MS conditions were nitrogen sheath gas (40 arbitrary units), nitrogen auxiliary gas (10 arbitrary units), spray



voltage (5.0 kV), capillary temperature (280 °C) and capillary voltage (30.0 V). The molecular ions of AT-III and IS were detected in the full-scan mode (m/z 50–500). The molecular ions $[M + H]^+$ and their fragmented ions were acquired at m/z 248.99–230.96 for AT-III and m/z 233.00–214.98 for IS. Moreover, the single oxygen atom-added metabolite of AT-III (AT-III-O) was detected at m/z 264.92–246.99 after the oral administration of AT-III, as previously reported.¹⁶ Data was processed using Xcalibur software (v. 2.1.0; Thermo Fisher Scientific, CA, USA).

Collection of rat plasma samples

AT-III (18 mg per rat) was administered to five SD rats and one rat was given a vehicle. AT-III was dissolved in 0.5% ethanol-contained saline (v/v). Blood samples (~0.4 mL) were collected from the jugular vein in heparinised tubes before oral administration (0 h), and at 0.17, 0.5, 1, 2, 4, 8 and 12 h after intragastric administration. The collected blood samples were immediately centrifuged at $16\,249 \times g$ for 10 min; 150 μ L aliquots of the supernatant plasma were transferred to clean tubes and stored at -20 °C until the analysis.

Preparation of plasma samples

The extraction efficiencies of the liquid–liquid extraction (LLE) and the protein precipitation methods were compared using the absolute area of the target compounds and IS. The peak areas of AT-III and IS obtained *via* LLE in ethyl acetate (EA) were 1.4-fold higher than those obtained using the protein precipitation method in methanol. Therefore, the LLE method was chosen for preparing the plasma samples due to its higher extraction efficiency, simplicity and reliability. A 150 μ L aliquot of the plasma sample was spiked with the IS solution (10 μ L) and of methanol (10 μ L), followed by the addition of EA (600 μ L). The extraction of the target compounds was performed by vortex mixing for 2 min at room temperature, followed by centrifuging at $16\,249 \times g$ for 10 min at 20 °C. The upper layer (EA) was then transferred to a clean 1.5 mL polypropylene tube and evaporated using a nitrogen gas blowing concentrator (MGS-2200; Eyela, Miyagi, Japan). The residue obtained after evaporation was reconstituted in methanol (100 μ L) and vortex mixed for 2 min, followed by centrifugation at $16\,249 \times g$ for 10 min at 20 °C. The supernatant was transferred to a glass vial and a 5 μ L aliquot was injected into the UPLC-ion trap MS system.

Statistical analysis

The relative area ratio of each compound was calculated using the following equation: Relative area ratio = the peak area of the target compound/the peak area of IS. The difference in the ratios between the single and APAP-combined groups were determined *via* two-tailed *t*-test (independent sample *t*-test) using Microsoft Excel (ver. 2014; Redmond, WA, USA). The differences were considered statistically significant at $p < 0.05$, $p < 0.01$, or $p < 0.001$.

Kinetics studies

The UV-vis spectra were recorded on a UV-visible spectrophotometer (Cary 8454; Agilent, Santa Clara, CA, USA) equipped with a temperature-controlled cuvette holder (UNISOKU Co., Ltd., Hirakata, Osaka, Japan). The reactions were followed by monitoring the UV-vis spectral changes of the reaction solutions at -40 °C. All reactions were run in triplicate, and the data reported represented the average of these reactions. The iron(IV)-oxo porphyrin π -cation radical species, $[(\text{tmp}^{+})\text{Fe}^{\text{IV}}(\text{O})]^+$ (1), was prepared as previously reported; briefly, $[\text{Fe}^{\text{III}}(\text{tmp})](\text{CF}_3\text{SO}_3)$ was treated with 2.4 equiv. of *m*-CPBA in a $\text{CH}_3\text{CN}/\text{CH}_2\text{Cl}_2$ (9 : 1) solvent mixture at -20 °C.⁵ The formation of the iron(IV)-oxo intermediates was confirmed *via* UV-vis spectrophotometry. Subsequently, appropriate amounts of AT-III were added to the reaction solutions. After the completion of the reactions, pseudo-first-order fitting of the kinetic data allowed us to determine the k_{obs} values. The resulting solution was directly injected into the HPLC for the identification and quantification of the reaction products. The products were identified by comparing the obtained retention times and mass patterns to those of known authentic samples. The hydroxylated of AT-III was confirmed *via* LC/MS analysis.

Cyclic voltammetry

Electrochemical measurements were performed on a CHI617B electrochemical analyzer (CH Instruments, Inc., Austin, TX, USA) in CH_3CN containing 0.10 M Bu_4NPF_6 (TBAPF₆) as the supporting electrolyte at 25 °C. A conventional three-electrode cell was used with a glassy carbon working electrode (surface area of 0.030 cm^2), a platinum wire as the counter electrode and an Ag/Ag^+ electrode as the reference electrode (in CH_3CN). The glassy carbon working electrode was routinely polished with BAS polishing alumina suspension and rinsed with acetone and acetonitrile before use. The measured potentials were recorded with respect to the Ag/Ag^+ (0.010 M) reference electrode (in CH_3CN).

DFT calculation

The geometric optimisation of AT-III, the one-electron oxidised AT-III and the 4th and 10th carbon oxidised AT-III were conducted with the starting structure taken from the known structure of AT-III and manually modified. DFT²² geometric optimisations and frequency calculations were performed at the B3LYP/6-31G level^{23–32} of theory using the Gaussian 16 package.³³ Solvent (water) effects were incorporated, even during geometry optimizations, through CPCM scheme as implemented in Gaussian 16.^{34,35} The energy evaluations were performed at the B3LYP/6-311+G** level^{29,36–44} on the structure obtained *via* B3LYP/6-31G.

Conclusions

We noted that both AT-III and its oxygenated form (AT-III-O) were detected in plasma samples collected from rats after the oral administration of AT-III. A catalytic reaction model using iron(IV)-oxo porphyrin, $[(\text{tmp}^{+})\text{Fe}^{\text{IV}}(\text{O})]^+$ (1), revealed that the



oxygenation of AT-III proceeded *via* H-atom abstraction and an oxygen rebound mechanism, with a second-order rate constant (k_2) of $2.8 \text{ M}^{-1} \text{ s}^{-1}$ at -20°C that was mediated by **1**. Theoretical calculations revealed that the oxygenation of AT-III by **1** occurred at the 4th and 10th carbon positions. Although the chemical reaction model revealed that the oxidation of APAP was faster than that of AT-III using **1**, we noted that the co-administration of APAP with AT-III did not affect the kinetic changes of AT-III and AT-III-O in the rat model. Given these findings, we theorised that the metabolism of AT-III involved CYP450 and other O_2 -activating metalloenzymes. The complexity of the metabolic pathways is highlighted in the present study and warrants more detailed investigations to determine its usefulness combinatorial medical applications.

Author contributions

Hanae Lim: methodology, validation, formal analysis, investigation, data curation, writing – original draft. Hyeri Jeon: methodology, formal analysis, data curation. Seungwoo Hong: methodology, validation, formal analysis, investigation, data curation, writing – original draft, writing – review & editing, supervision, project administration, funding acquisition. Jung-Hoon Kim: methodology, validation, formal analysis, investigation, data curation, writing – original draft, writing – review & editing, supervision.

Conflicts of interest

There are no conflicts to declare.

Acknowledgements

This work was supported by National Research Foundation of Korea (NRF) grant funded by the Korea government (MSIT; the Ministry of Science and ICT) (No. 2020R1C1C1008886 to S. Hong). The authors thank the Korean Herbarium of Standard Herbal Resources, Korea Institute of Oriental Medicine for providing the sample materials.

Notes and references

- J. B. Liu, D. Chen, T. T. Bao, F. T. Fan and C. Yu, *Front. Pharmacol.*, 2020, **10**, 1505.
- M. Wang, R. Hu, Y. Wang, L. Liu, H. You, J. Zhang, X. Wu, T. Pei, F. Wang, L. Lu, W. Xiao and L. Wei, *Oxid. Med. Cell. Longevity*, 2019, **2019**, 1875471.
- K. C. Zhou, J. Chen, J. Y. Wu, Q. Y. Wu, C. Q. Jia, Y. X. Z. Xu, L. Chen, W. Tu, G. Yang, J. Kong, J. Kou and S. Jiang, *Phytomedicine*, 2019, **59**, 152922.
- G. Q. Ji, R. Q. Chen and L. Wang, *Immunopharmacol. Immunotoxicol.*, 2016, **38**, 98–102.
- J. H. Kim, Y. Lee, G. Lee, E. J. Doh and S. Hong, *ACS Omega*, 2018, **3**, 14833–14840.
- F. P. Guengerich, *AAPS J.*, 2006, **8**, E101–E111.
- P. Josephy, F. P. Guengerich and J. O. Miners, *Drug Metab. Rev.*, 2005, **37**, 575–580.
- J. Olah, A. J. Mulholland and J. N. Harvey, *Proc. Natl. Acad. Sci. U. S. A.*, 2011, **108**, 6050–6055.
- P. C. Nair, R. A. McKinnon and J. O. Miners, *Drug Metab. Rev.*, 2016, **48**, 434–452.
- A. W. Munro, H. M. Girvan and K. J. McLean, *Nat. Prod. Rep.*, 2007, **24**, 585–609.
- L. Ji, A. S. Faponle, M. G. Quesne, M. A. Sainna, J. Zhang, A. Franke, D. Kumar, R. van Eldik, W. Li and S. P. de Visser, *Chem.–Eur. J.*, 2015, **21**, 9083–9092.
- C. Fertinger, N. Hessenauer-Ilicheva, A. Franke and R. van Eldik, *Chem.–Eur. J.*, 2009, **15**, 13435–13440.
- M. Oszajca, A. Franke, A. Drzewiecka-Matuszek, M. Brindell, G. Stochel and R. van Eldik, *Inorg. Chem.*, 2014, **53**, 2848–2857.
- C. M. Chapman, J. M. Pruneau, C. A. Laverack, A. S. Dutton and G. B. Jones, *Appl. Catal., A*, 2015, **510**, 204–215.
- F. G. C. Reinhard and S. P. de Visser, *Inorganics*, 2017, **5**, 77.
- Z. Jiang, C. Peng, W. Huang, B. Wu, D. Zhang, H. Ouyang, Y. Feng and S. Yang, *J. Chromatogr. Sci.*, 2019, **57**, 163–176.
- S. Spinozzi, C. Colliva, C. Camborata, M. Roberti, C. Ianni, F. Neri, C. Calvarese, A. Lisotti, G. Mazzella and A. Roda, *J. Nat. Prod.*, 2014, **77**, 766–772.
- Y. Bai, W. Peng, C. Yang, W. Zou, M. Liu, H. Wu, L. Fan, P. Li, X. Zeng and W. Su, *Front. Pharmacol.*, 2020, **11**, 364.
- D. W. Potter and J. A. Hinson, *J. Biol. Chem.*, 1987, **262**, 966–973.
- R. A. Marcus, *Angew. Chem., Int. Ed. Engl.*, 1993, **32**, 1111–1121.
- W. L. F. Armarego and C. L. L. Chai, *Purification of Laboratory Chemicals*, Pergamon Press, Oxford, 6th edn, 2009.
- W. Kohn and L. J. Sham, *Phys. Rev.*, 1965, **140**, A1133–A1138.
- R. Ditchfield, W. J. Hehre and J. A. Pople, *J. Chem. Phys.*, 1971, **54**, 724–728.
- W. J. Hehre, R. Ditchfield and J. A. Pople, *J. Chem. Phys.*, 1972, **56**, 2257–2261.
- P. C. Hariharan and J. A. Pople, *Theor. Chem. Acc.*, 1973, **28**, 213–222.
- P. C. Hariharan and J. A. Pople, *Mol. Phys.*, 1974, **27**, 209–214.
- M. S. Gordon, *Chem. Phys. Lett.*, 1980, **76**, 163–168.
- M. M. Francl, W. J. Pietro, W. J. Hehre, J. S. Binkley, D. J. DeFrees, J. A. Pople and M. S. Gordon, *J. Chem. Phys.*, 1982, **77**, 3654–3665.
- R. C. Binning Jr and L. A. Curtiss, *J. Comput. Chem.*, 1990, **11**, 1206–1216.
- J.-P. Blaudeau, M. P. McGrath, L. A. Curtiss and L. Radom, *J. Chem. Phys.*, 1997, **107**, 5016–5021.
- V. A. Rassolov, J. A. Pople, M. A. Ratner and T. L. Windus, *J. Chem. Phys.*, 1998, **109**, 1223–1229.
- V. A. Rassolov, M. A. Ratner, J. A. Pople, P. C. Redfern and L. A. Curtiss, *J. Comput. Chem.*, 2001, **22**, 976–984.
- M. J. Frisch, G. W. Trucks, H. B. Schlegel, G. E. Scuseria, M. A. Robb, J. R. Cheeseman, G. Scalmani, V. Barone, G. A. Petersson, H. Nakatsuji, X. Li, M. Caricato, A. V. Marenich, J. Bloino, B. G. Janesko, R. Gomperts, B. Mennucci, H. P. Hratchian, J. V. Ortiz, A. F. Izmaylov, J. L. Sonnenberg, D. Williams-Young, F. Ding, F. Lipparini, F. Egidi, J. Goings, B. Peng, A. Petrone, T. Henderson,



- D. Ranasinghe, V. G. Zakrzewski, J. Gao, N. Rega, G. Zheng, W. Liang, M. Hada, M. Ehara, K. Toyota, R. Fukuda, J. Hasegawa, M. Ishida, T. Nakajima, Y. Honda, O. Kitao, H. Nakai, T. Vreven, K. Throssell, J. A. Montgomery Jr, J. E. Peralta, F. Ogliaro, M. J. Bearpark, J. J. Heyd, E. N. Brothers, K. N. Kudin, V. N. Staroverov, T. A. Keith, R. Kobayashi, J. Normand, K. Raghavachari, A. P. Rendell, J. C. Burant, S. S. Iyengar, J. Tomasi, M. Cossi, J. M. Millam, M. Klene, C. Adamo, R. Cammi, J. W. Ochterski, R. L. Martin, K. Morokuma, O. Farkas, J. B. Foresman and D. J. Fox, *Gaussian 16, Revision B.01*, Gaussian, Inc., Wallingford CT, 2016.
- 34 V. Barone and M. Cossi, *J. Phys. Chem. A*, 1998, **102**, 1995–2001.
- 35 M. Cossi, N. Rega, G. Scalmani and V. Barone, *J. Comput. Chem.*, 2003, **24**, 669–681.
- 36 A. D. McLean and G. S. Chandler, *J. Chem. Phys.*, 1980, **72**, 5639–5648.
- 37 K. Raghavachari, J. S. Binkley, R. Seeger and J. A. Pople, *J. Chem. Phys.*, 1980, **72**, 650–654.
- 38 J.-P. Blaudeau, M. P. McGrath, L. A. Curtiss and L. Radom, *J. Chem. Phys.*, 1997, **107**, 5016–5021.
- 39 A. J. H. Wachters, *J. Chem. Phys.*, 1970, **52**, 1033–1036.
- 40 P. J. Hay, *J. Chem. Phys.*, 1977, **66**, 4377–4384.
- 41 K. Raghavachari and G. W. Trucks, *J. Chem. Phys.*, 1989, **91**, 1062–1065.
- 42 M. P. McGrath and L. Radom, *J. Chem. Phys.*, 1991, **94**, 511–516.
- 43 L. A. Curtiss, M. P. McGrath, J.-P. Blaudeau, N. E. Davis, R. C. Binning Jr and L. Radom, *J. Chem. Phys.*, 1995, **103**, 6104–6113.
- 44 T. Clark, J. Chandrasekhar, G. W. Spitznagel and P. v. R. Schleyer, *J. Comput. Chem.*, 1983, **4**, 294–301.

